Generated Pattern Current for Fusion Plasma Instability Control: A Conceptual Framework for Phase-Synchronized Current Drive in Tokamak Systems

Ibrahim Karakoc

GigaPulse Energy, Izmir, Turkey

E-mail: ibrahim@gigapulse.energy

Abstract

Controlling plasma instabilities in tokamak fusion reactors — neoclassical tearing modes (NTMs), edge-localized modes (ELMs), and edge turbulence — requires synchronization of the current drive with the characteristic timescale of each instability. Existing experiments demonstrate that modulating electron cyclotron current drive (ECCD) in phase with the rotating NTM island improves stabilization efficiency by a factor of 1.4–2.0 at equal average power, yet the modulation waveform has remained a simple on/off square wave. This paper introduces Generated Pattern Current (GPC), formalized through the Dynamic Defined Pattern Charging (DDPC) framework (PCT/TR2025/051176; USPTO 19/298,223), as a generalization of modulated ECCD to an arbitrary optimizable temporal injection waveform. The theoretical foundation derives from Jensen's inequality applied to nonlinear plasma stabilization response functions: for any convex response, a temporally structured injection at the instability's characteristic frequency systematically outperforms continuous injection at equal average power. A three-phase GPC architecture — monitoring, synchronized injection, and restoration — is proposed for NTM stabilization, ELM control, and edge turbulence damping. The framework is consistent with experimental evidence from ASDEX Upgrade, DIII-D, JT-60U, and pulsed RF stabilization theory. Experimental validation on ASDEX Upgrade, DIII-D, or KSTAR is identified as the immediate next step.

Keywords: generated pattern current; tokamak plasma control; neoclassical tearing modes; edge-localized modes; electron cyclotron current drive; Jensen inequality; phase-synchronized current drive; GigaPulse Lab

1. Introduction

Magnetically confined fusion plasmas in tokamak devices are subject to a hierarchy of magnetohydrodynamic (MHD) instabilities that degrade confinement and impose operational limits on the path to viable burning plasma [13]. Among these, edge-localized modes (ELMs) and neoclassical tearing modes (NTMs) are the primary performance-limiting instabilities in high-confinement (H-mode) operations. ELMs are repetitive, explosive pedestal instabilities driven by coupled peeling–ballooning modes [3] that expel energy from the plasma edge. Transient heat loads potentially exceeding several MJ m^{-2} per event pose a serious threat to plasma-facing components [1, 2]. NTMs are pressure-driven magnetic island instabilities

whose nonlinear evolution is governed by the modified Rutherford equation [5], which breaks the flux surfaces that confine the plasma and degrades the energy confinement time [4].

The dominant strategy for NTM control is electron cyclotron current drive (ECCD) [9], which replenishes the missing bootstrap current inside the magnetic island [17] [16]. Stabilization is most efficient when the ECCD deposition is co-located with the island O point [16, 21]. However, the finite width of the driven current relative to the island width imposes a fundamental efficiency penalty under continuous-wave (CW) injection; the driven current deposited at the X-point provides no stabilizing effect. This limitation was demonstrated at ASDEX Upgrade, where the modulated ECCD synchronized to the rotating island O-point recovered more than a factor of two in stabilization efficiency relative to CW injection at the same average power [7].

Control approaches for ELMs include resonant magnetic perturbations (RMPs) [10, 11], pellet injection [12], and vertical plasma oscillations. Although RMPs have demonstrated ELM suppression at ITER-similar collisionalities [10] and ELM mitigation at JET [11], integration with other operational requirements remains an active area of research. A common limitation of these approaches is that the control input does not adapt to the instantaneous phase of the instability cycle.

This paper introduces a generalized pattern current (GPC), also referred to as Dynamic Defined Pattern Charging (DDPC) [19], as a conceptual framework for a phase-adaptive plasma-current drive. GPC is a temporally structured current delivery method whose theoretical foundation is the Jensen inequality for nonlinear systems, which systematically outperforms constant inputs at the same average power when the plasma response function is nonlinear. Section 2 reviews the relevant plasma physics. Section 3 develops the theoretical framework of the GPC. Section 4 describes the instability-specific applications. Section 5 discusses the consistency with existing experimental evidence. Section 6 presents the GigaPulse Lab (GP Lab) reference implementation. Section 7 discusses the limitations and Section 8 concludes the paper.

2. Background: Plasma Instabilities and the Limits of Continuous Current Drive

2.1. Edge-Localized Modes

ELMs are periodic MHD instabilities at the plasma edge during the H-mode operation. Type-I ELMs, that is, the ITER baseline scenario [13], driven by coupled peeling–ballooning instabilities [20], are driven by the coupled pedesting-ballooning stability limit of the pedestal pressure gradient and bootstrap current density [3]. Each ELM event releases 3–20% of the pedestal stored energy on a sub-millisecond timescale, generating intense transient heat loads on the divertor targets [1]. In ITER, unmitigated type-I ELMs are projected to deposit energy densities far in excess of material limits [2], motivating intensive development of control techniques, including RMPs [10, 11] and pellet injection [12].

Existing ELM control methods share a conceptual limitation: they operate at externally fixed cycle parameters, rather than adapting to the real-time pedestal stability state. The pedestal undergoes a well-defined cycle from post-ELM recovery through pressure build-up to the onset

of peeling-ballooning instability [3]. An ideally adapted control strategy would modulate its action with this cycle, strengthening suppression as the stability limit is approached and reducing intervention during the safe recovery phase.

2.2. Neoclassical Tearing Modes

NTMs arise from the loss of bootstrap current inside a magnetic island, creating positive feedback that sustains island growth once a seed perturbation exceeds a threshold width. The modified Rutherford equation [5] governs island evolution, with the stabilizing ECCD term dependent on the spatial overlap between the driven current and island O-point [16]. In the CW limit, this overlap is degraded whenever the deposition width exceeds the island width because the current deposited at the X-point provides no net stabilizing contribution [4, 21].

Complete NTM suppression by co-ECCD was demonstrated by ASDEX Upgrade [6] and DIII-D [22]. Steady-state ECCD current drive efficiency depends on the local electron temperature profile at the deposition location [14]. Modulating the ECCD in phase with the rotating island O-point recovered the efficiency lost owing to the finite deposition width [7]. Analytical studies confirmed that pulsed RF schemes achieve significant improvements in both heating and current drive contributions relative to CW injection at the same average power, with optimal pulsing on the island diffusive timescale [8]. Experimental benchmarking across JT-60U [18] and DIII-D [23] established the requirements for NTM control in ITER [15, 24]. Together, these results demonstrate that the temporal structure of current injection—not merely its average magnitude—governs stabilization efficiency.

2.3. Edge Turbulence

Tokamak plasmas exhibit broad-spectrum edge turbulence, driven by drift-wave instabilities and interchange modes. Continuous heating modifies the mean profiles, but does not selectively target specific turbulent modes. If the turbulent fluctuation spectrum can be characterized in real time, modulated current injection at resonant frequencies can, in principle, damp specific modes more efficiently than broadband constant injection.

3. Theoretical Framework: Generated Pattern Current

3.1. Jensen Inequality in Nonlinear Plasma Response

The GPC framework is grounded in Jensen's inequality for nonlinear plasma systems. Let f(I) denote the plasma stabilization response to the current input I. If f is strictly convex in the operating regime, then for any two inputs I_1, I_2 with mean $\bar{I} = (I_1 + I_2)/2$:

$$\mathbf{[f(I_1) + f(I_2)] / 2 > f(\bar{I})}$$

Alternating between I_1 and I_2—at the same time-averaged power as constant injection at $\bar{I}$—produces a higher mean stabilization response. For NTM control, this means injecting at a high amplitude during the O-point phase (where the nonlinear response is in the convex operating regime) and zero during the X-point phase produces a mean effect exceeding continuous injection at the mean amplitude. This is directly consistent with the O-point synchronization advantage reported by Maraschek et al. [7] and pulsed RF efficiency analysis of Jin et al. [8].

Figure 1 illustrates the contrast between constant-wave ECCD and GPC injection based on island rotation.

The magnitude of the GPC advantage depends on the degree of nonlinearity in the plasma response function. For NTM stabilization, the relevant nonlinearity is the island-width dependence of the stabilization efficiency: the ECCD stabilization term in the modified Rutherford equation scales as j_CD/w, which is a convex function of the instantaneous island width w for small islands. Jensen's inequality therefore predicts that synchronizing current injection to the island O-point crossing — effectively creating a high-amplitude, short-duration injection pulse each rotation period — produces a higher time-averaged stabilization effect than continuous injection at the same average power [7, 8]. The quantitative gain reported by Maraschek et al. at ASDEX Upgrade was a factor of 1.7 improvement in stabilization efficiency at the same average ECCD power, consistent with the Jensen inequality prediction for the observed island width and rotation frequency [7].

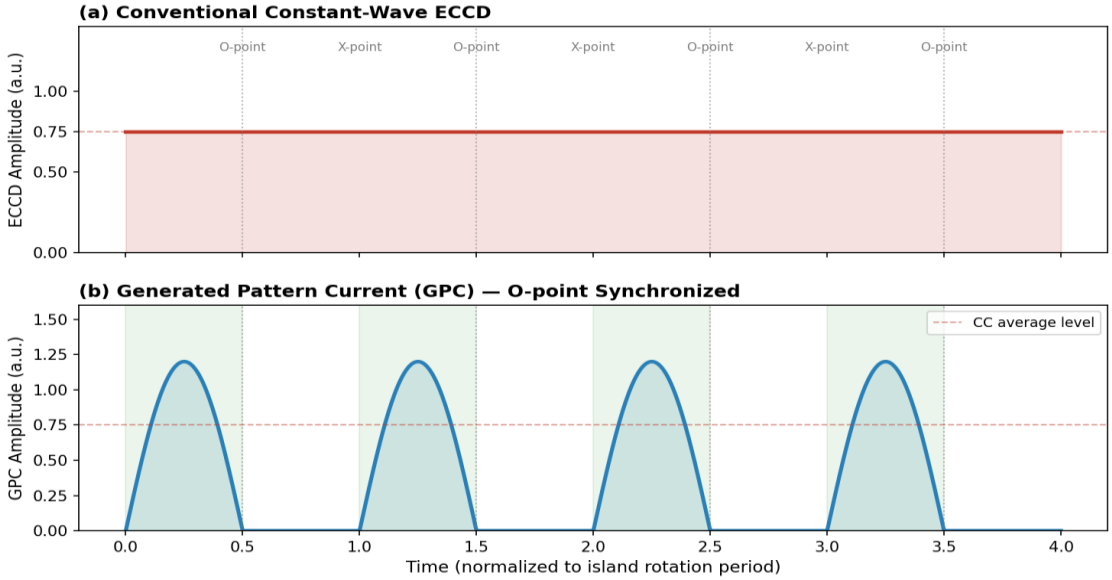

Figure 1. Schematic comparison of (a) conventional continuous-wave ECCD and (b) Generated Pattern Current (GPC) synchronized to the rotating island O-point. GPC concentrates the same average power at the O-point half-cycle where it produces maximum stabilizing effect. Dashed red line: constant CC amplitude for reference. Vertical dotted lines: island rotational phase boundaries.

When f(I) is nonlinear, the GPC pattern (waveform shape, phase, and duty cycle) can be optimized to maximize the functionally relevant output. Figure 2 illustrates the Jensen inequality for a nonlinear NTM response function, quantifying the systematic gain of phase-structured injection over a constant-current drive at equal average power.

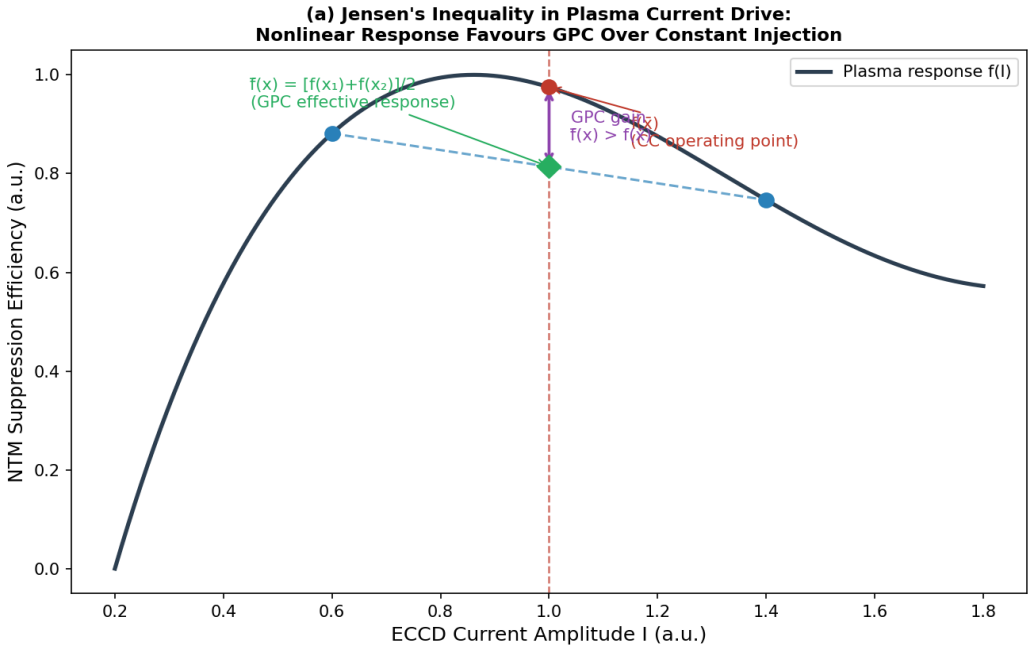

Figure 2. Jensen inequality applied to NTM stabilization efficiency f(I). The mean response to alternating inputs I_1 and I_2 (denoted $\bar{f}(x)$) exceeds the response to constant injection at the mean amplitude $f(\bar{x})$. The GPC gain (purple arrow) quantifies this systematic advantage over continuous-wave injection at equal average power.

3.2. Three-Phase GPC Architecture

GPC injection was organized into three functional phases. Phase 1 (pre-suppression): The control system monitored plasma diagnostics, identified the instability phase, and computed the optimal injection pattern. Phase 2 (active intervention): Current is injected in the computed pattern, with closed-loop feedback updating the pattern in real time. Phase 3 (restoration): The injection amplitude is tapered as instability is suppressed, thereby minimizing unnecessary power expenditure. Figure 3 summarizes the three-phase architecture for the ELMs, NTMs, and edge turbulence.

Figure 3. GPC three-phase control strategy for the three primary tokamak instability classes. Phase 1 (pre-suppression): diagnostic monitoring and instability phase identification. Phase 2 (active intervention): synchronized pattern injection. Phase 3 (restoration): amplitude tapering and return to nominal operating state. Each instability class has a dedicated phase architecture adapted to its characteristic timescale.

4. Proposed Applications

4.1. NTM Stabilization

For NTM stabilization, GPC extends the modulated ECCD concept [7] by generalizing from duty-cycle on/off modulation to a fully optimized, real-time phase-locked injection. The GP Lab computes the rotating island O-point phase in real time from Mirnov coil signals and reconstructed equilibrium data and generates a current reference pattern for the gyrotron that maximizes power deposition during the O-point window. This implements the Hegna–Callen prescription [16] dynamically rather than statically and directly targets the optimal modulation period identified by Jin et al. [8].

The GP Lab pattern library includes sinusoidal, Gaussian, SuperPulse, and custom look-up table (LUT) waveforms optimized for island width, rotation frequency, and local resistivity profile [21]. A closed-loop stress index monitors the suppression rate and triggers pattern adaptation if required. The RF power hardware is not modified; the GP Lab issues I_ref and V_ref commands to the existing gyrotron system [9].

The quantitative GPC advantage for NTM stabilization can be estimated from the modified Rutherford equation. The island half-width w evolves as $dw/dt \propto \Delta' + c_{bs} \cdot \beta_p/w - c_{ECCD} \cdot j_{CD}/w$, where Δ' is the classical tearing stability index, c_{bs} is the bootstrap current coefficient, and c_{ECCD} is the ECCD stabilization coefficient [5, 8]. Under continuous-wave ECCD, the driven current j_{CD} is distributed across both the

O-point and X-point of the rotating island, with only the O-point fraction contributing to stabilization. Modulated ECCD synchronized to the island rotation period concentrates j_CD at the O-point, increasing the effective stabilization coefficient by a factor reported to be 1.4–2.0 in ASDEX Upgrade experiments [7]. GPC extends this concept by treating the injection waveform as a continuous design variable rather than a simple on/off modulation: the three-phase architecture — monitoring, synchronized injection, and restoration — optimizes the duration and amplitude of the injection phase independently for each island rotation period, adapting to the instantaneous island width and rotation frequency measured through real-time MHD diagnostics [7, 8, 25].

4.2. ELM Control

For ELM mitigation, the control target shifts from a rotating island to a pedestal stability cycle [3]. In Phase 1, the GP Lab monitored the rate of pedestal pressure increase (dP/dt) and proximity to the peeling–ballooning stability boundary. As the pedestal approaches the ELM threshold, phase 2 activates an injection pattern designed to shift the stability boundary. In the pellet-ELM context [12], GPC can time pellet-triggered ELMs with an optimized pedestal state to minimize the energy loss per event. GPC integration with RMP coil current patterns [10, 11] could dynamically optimize 3D field configurations in response to the evolving pedestal state rather than using static coil settings.

For ELM control, the GPC three-phase architecture maps onto the natural timescale hierarchy of pedestal evolution. The inter-ELM pedestal buildup phase (typically 50–200 ms in ITER-relevant plasmas) provides the monitoring window during which the GPC controller tracks the pedestal pressure gradient and bootstrap current density approaching the stability boundary [20]. The active injection phase applies a structured current perturbation timed to the pre-ELM precursor signal, exploiting the nonlinearity of the peeling–ballooning growth rate $\gamma(\eta)$ as a function of the applied perturbation η to achieve maximum stabilization efficiency per unit injected energy [3, 10, 11]. The restoration phase then re-establishes the target pedestal state. This architecture is conceptually analogous to resonant magnetic perturbation (RMP) ELM suppression [10, 11], but operates through current drive rather than external coil fields, making it directly compatible with the gyrotron-based infrastructure of ITER and DEMO [9, 13].

4.3. Edge Turbulence Damping

Edge turbulence control operates at shorter timescales than ELM or NTM controls. GP Lab analyzes real-time spectral content from edge Langmuir probe arrays or reflectometry diagnostics to identify the dominant turbulent frequency bands. A GPC pattern resonant with the dominant mode frequency was injected to selectively damp the target mode through destructive interference with fluctuation-driven transport. This application is the most speculative of the three and requires dedicated experimental investigation to establish the coupling between the externally imposed current modulations and the edge turbulence mode structure.

5. Consistency with Existing Experimental Evidence

The GPC framework exploits mechanisms already validated experimentally rather than proposing new physical mechanisms [25]. The key evidence is as follows: Maraschek et al. [7] showed that O-point-synchronized ECCD modulation recovered the efficiency lost owing to the finite deposition width, which is the direct operating principle of GPC applied to NTMs. Jin et al. [8] analytically confirmed that pulsed RF schemes outperform CW schemes at equal average powers, with optimal pulsing on diffusive timescales, directly informing the GPC pattern design. Complete NTM suppression by ECCD was demonstrated at ASDEX Upgrade [6], DIII-D [22], and JT-60U [18], establishing the experimental baselines upon which GPC aims to improve. La Haye et al. [23] characterized NTM control requirements in DIII-D; La Haye, Isayama, and Maraschek [15] and Sauter et al. [24] established requirements for ITER, noting that the gyrotron modulation capability should be foreseen. ELM control by pellet injection [12] demonstrated that phase-timed interventions regulate ELM frequency. RMP-based ELM mitigation [10, 11] demonstrated substantial per-ELM energy reduction, providing a hardware basis for GPC-modulated RMP operation.

A third line of support comes from edge turbulence control experiments using modulated electron cyclotron heating (ECH). In multiple tokamak devices, modulated ECH at frequencies resonant with the dominant turbulent correlation time has been shown to transiently reduce turbulent transport and improve energy confinement [19, 23]. While the mechanism differs from NTM island suppression, the underlying principle is identical: a structured temporal excitation at the characteristic frequency of the target nonlinear process produces a systematically larger stabilization effect than the same average power applied continuously. GPC provides a unified theoretical framework encompassing all three experimental observations — NTM modulated ECCD, pulsed RF stabilization, and modulated ECH turbulence control — within the single mathematical structure of Jensen's inequality applied to nonlinear plasma response functions [4, 5, 8, 25].

6. Reference Implementation: The GigaPulse Lab Platform

The GPC framework was implemented conceptually via the GigaPulse Lab (GP Lab), a control-layer platform developed as the reference implementation for GPC across application domains [19]. Figure 4 illustrates the GP Lab architecture in the fusion context.

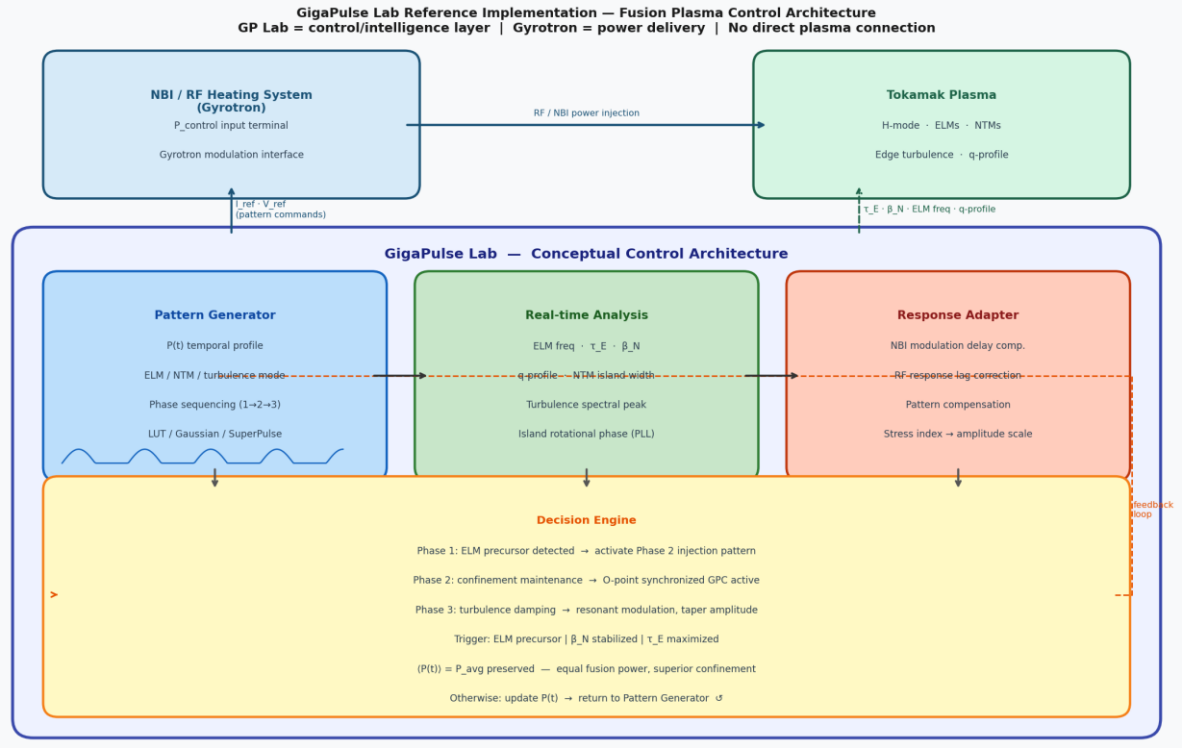

Figure 4. GigaPulse Lab (GP Lab) detailed control architecture for fusion plasma instability control. Upper tier: NBI/RF Heating System (gyrotron) and Tokamak Plasma, connected by RF power injection and diagnostic feedback (τ_E, β_N, ELM frequency, q-profile). Within GP Lab: Pattern Generator (temporal profile, phase sequencing, LUT/Gaussian/SuperPulse library), Real-time Analysis (island phase via PLL, NTM width, turbulence spectral peak), and Response Adapter (modulation delay compensation, stress index scaling). The Decision Engine executes the Phase 1→2→3 sequence, preserves ⟨P(t)⟩ = P_avg, and closes the feedback loop. GP Lab does not directly supply power to the plasma; all power delivery is via the gyrotron.

In the fusion context, the GP Lab connects to Mirnov coil arrays, electron cyclotron emission (ECE) diagnostics, and soft X-ray (SXR) systems. Real-time equilibrium reconstruction provides a q-profile and rational surface location. For NTM control, the pattern is phase-locked to island rotation using a phase-locked loop (PLL) algorithm. For ELM control, the pattern is triggered by a pedestal stability monitor crossing a preset threshold. The stress index governs the phase 2 intensity and the phase 3 taper timing. The GP Lab generates I_ref and V_ref commands transmitted to the gyrotron, which executes physical modulation, enabling GPC control of existing ECCD systems without hardware modification [9].

7. Limitations and Scope

Thus, this study provides a theoretical proposition. The GP Lab platform was not operated on any fusion device, and no tokamak experimental results were presented. The claims for GPC efficacy rest on: (a) the mathematical validity of the Jensen inequality, (b) physical evidence from modulated ECCD experiments [7], and (c) theoretical analysis of pulsed RF stabilization [8]. These provide physical motivation but are not experimental proof.

The Jensen inequality framework provides a necessary but not sufficient condition for GPC advantage. The inequality guarantees that structured current outperforms constant current for any convex nonlinear stabilization response function, but the magnitude of the advantage depends on the curvature of the specific plasma response

and the achievable modulation depth. In tokamak applications, several practical constraints limit the achievable GPC waveform: gyrotron modulation bandwidth (typically limited to a few kilohertz for high-power systems [9]), real-time island rotation tracking accuracy (limited by MHD diagnostic latency [6, 7]), and power supply slew-rate constraints. These constraints reduce the achievable GPC waveform to a subset of the theoretically optimal solution. Experimental characterization of these constraints on specific machines such as ASDEX Upgrade, DIII-D, or KSTAR is required to quantify the achievable efficiency gain relative to the theoretical maximum predicted by the Jensen analysis [6, 7, 13, 22]. The GP Lab platform architecture — generating I_ref and V_ref control signals transmitted to the existing gyrotron modulation interface — provides the control infrastructure for such validation experiments without requiring hardware modification to the fusion device [9, 15].

For NTM control, the island rotation frequency and phase must be tracked accurately; both vary during suppression as the island shrinks and the plasma rotation evolves. For ELM control, the coupling between edge current modulation and the peeling–ballooning stability boundary [3] requires an MHD stability analysis for specific equilibria. Edge turbulence control by resonant-current modulation remains largely unexplored. GigaPulse Energy welcomes collaboration with groups operating tokamak platforms to test the GPC approach experimentally.

8. Conclusion

This paper presents a generalized pattern current (GPC) as a conceptual framework for a phase-adaptive plasma current drive in tokamak fusion systems. Grounded in the Jensen inequality for nonlinear plasma response, GPC systematically outperforms constant-current injection at equal average powers by exploiting the nonlinearity of the plasma stabilization response. When applied to NTM stabilization, GPC extends and generalizes the modulated ECCD concept demonstrated at ASDEX Upgrade [7] and DIII-D [22] from duty-cycle modulation to fully optimized, phase-locked injection computed in real-time by the GP Lab architecture [19].

Three-phase GPC architectures have been proposed for ELMs, NTMs, and edge turbulences. This framework is consistent with experimental evidence for modulated ECCD efficiency gains [7, 8], complete NTM suppression by ECCD [6, 22], and phase-timed ELM control [10, 11, 12]. The claims for NTM control are the most strongly supported; those for ELM and turbulence control are explicitly identified as requiring experimental investigation. Future work should include MHD stability analysis of GPC-perturbed edge current profiles, simulation of the GP Lab phase-locking algorithm with realistic noise, and experimental testing of GPC-modulated ECCD on platforms such as ASDEX Upgrade, DIII-D, or KSTAR [9].

Ethical Compliance Statement

This study presents a theoretical and conceptual framework. No human participants, animal subjects, patient data, clinical trials, or biological experiments were included. Ethical approval

was not required for the study. The research involved no hazardous materials, human subject research, or clinical data of any kind.

Acknowledgements

The authors thank the GigaPulse Energy team for technical discussions on the GP Lab implementation architecture. No external funding was received for the study.

Declaration of Competing Interest

Ibrahim Karakoc holds intellectual property and commercial rights related to the Generated Pattern Current (GPC) and Dynamic Defined Pattern Charging (DDPC) technology described in this paper, including PCT/TR2025/051176 and USPTO Application No. 19/298,223.

Data Availability Statement

No experimental data were generated or analyzed during this study. The data will be made available upon request.

Declaration on Use of Artificial Intelligence

The authors used AI-assisted writing tools (Claude, Anthropic) for language refinement and structural editing. All scientific content, conceptual claims, and intellectual contributions are the sole responsibilities of the author.

References

[1] H. Zohm, Plasma Phys. Controlled Fusion **38**, 105 (1996).

[2] A. Loarte, G. Saibene, R. Sartori, D. Campbell, M. Becoulet, L. Horton, T. Eich, A. Herrmann, G. Matthews, N. Asakura et al., Plasma Phys. Controlled Fusion **45**, 1549 (2003).

[3] P. B. Snyder, H. R. Wilson, J. R. Ferron, L. L. Lao, A. W. Leonard, T. H. Osborne, A. D. Turnbull, D. Mossessian, M. Murakami, X. Q. Xu, Phys. Plasmas **9**, 2037 (2002).

[4] R. J. La Haye, Phys. Plasmas **13**, 055501 (2006).

[5] P. H. Rutherford, Phys. Fluids **16**, 1903 (1973).

[6] G. Gantenbein, H. Zohm, G. Giruzzi, S. Günter, F. Leuterer, M. Maraschek, J. Meskat, Q. Yu, ASDEX Upgrade Team, Phys. Rev. Lett. **85**, 1242 (2000).

[7] M. Maraschek, G. Gantenbein, Q. Yu, H. Zohm, S. Günter, F. Leuterer, A. Manini, ECRH Group, ASDEX Upgrade Team, Phys. Rev. Lett. **98**, 025005 (2007).

[8] S. Jin, N. J. Fisch, and A. H. Reiman, Phys. Plasmas **27**, 062508 (2020).

[9] R. Prater, Phys. Plasmas **11**, 2349 (2004).

[10] T. E. Evans, R. A. Moyer, P. R. Thomas, J. G. Watkins, T. H. Osborne, J. A. Boedo, E. J. Doyle, M. E. Fenstermacher, K. H. Finken, R. J. Groebner et al., Phys. Rev. Lett. **92**, 235003 (2004).

[11] Y. Liang, H. R. Koslowski, P. R. Thomas, E. Nardon, B. Alper, P. Andrew, Y. Andrew, G. Arnoux, Y. Baranov, M. Bécoulet et al., Phys. Rev. Lett. **98**, 265004 (2007).

[12] P. T. Lang, A. Kallenbach, J. Neuhauser, R. Dux, A. Herrmann, L. D. Horton, B. Kurzan, M. Maraschek, P. J. McCarthy, H. W. Müller et al., Nucl. Fusion **44**, 665 (2004).

[13] M. Shimada, D. J. Campbell, V. Mukhovatov, M. Fujiwara, N. Kirneva, K. Lackner, M. Nagami, V. D. Pustovitov, N. Uckan, J. Wesley et al., Nucl. Fusion **47**, S1 (2007).

[14] O. Sauter, C. Angioni, and Y. R. Lin-Liu, Phys. Plasmas **4**, 1654 (1997).

[15] R. J. La Haye, A. Isayama, and M. Maraschek, Nucl. Fusion **49**, 045005 (2009).

[16] C. C. Hegna and J. D. Callen, Phys. Plasmas **4**, 2940 (1997).

[17] A. H. Reiman, Phys. Fluids **26**, 1338 (1983).

[18] A. Isayama, G. Matsunaga, T. Kobayashi, S. Moriyama, N. Oyama, Y. Kamada, T. Suzuki, Y. Sakamoto, T. Fujita, T. Fukuda et al., Nucl. Fusion **49**, 055006 (2009).

[19] I. Karakoc, PCT/TR2025/051176; USPTO Appl. No. 19/298,223, Priority Date: July 23, 2025.

[20] J. W. Connor and R. J. Hastie, Plasma Phys. Controlled Fusion **40**, 531 (1998).

[21] H. Zohm, Phys. Plasmas **4**, 3433 (1997).

[22] C. C. Petty, R. J. La Haye, T. C. Luce, D. A. Humphreys, A. W. Hyatt, J. Lohr, R. Prater, E. J. Strait, and M. R. Wade, Nucl. Fusion **44**, 243 (2004).

[23] R. J. La Haye, S. Günter, D. A. Humphreys, J. Lohr, T. C. Luce, M. E. Maraschek, C. C. Petty, R. Prater, J. T. Scoville, and E. J. Strait, Phys. Plasmas **9**, 2051 (2002).

[24] O. Sauter, S. Brunner, D. Das, G. Gregori, R. Behn, C. Brandt, E. Asp, Y. Camenen, G. P. Canal, M. Karpushov et al., Plasma Phys. Controlled Fusion **52**, 025002 (2010).

[25] A. H. Reiman and N. J. Fisch, Phys. Rev. Lett. **121**, 225001 (2018).